RESEARCH ARTICLE | JULY 06 2023

Perspective on edge fracture

San To Chan ✉ 📵 ; Stylianos Varchanis; Simon J. Haward 📵 ; Amy Q. Shen 📵

Check for updates

CrossMark

View Online

Export Citation

Related Content

Prevention of edge fracture using a nontoxic liquid metal sealant

Physics of Fluids (January 2023)

Mathematics and rheology: The 1958 Bingham Medal Address

Physics Today (May 1959)

Inferring meaningful relaxation spectra from experimental data

Journal of Rheology (May 2014)

Perspective on edge fracture

San To Chan,[a)] Stylianos Varchanis, Simon J. Haward, and Amy Q. Shen

Micro/Bio/Nanofluidics Unit, Okinawa Institute of Science and Technology Graduate University, Onna, Okinawa 904-0495, Japan

Abstract

Edge fracture is a viscoelastic instability characterized by the sudden indentation of a fluid's free surface when the fluid is subjected to a high enough shear rate. During shear rheometry, the fracture can invade the fluid sample, decreasing its contact area with the rheometer fixture and rendering the measurement of viscosity and normal stresses at high-shear rates invalid. Edge fracture can also induce apparent shear banding in the fluid, complicating the interpretation of experimental results. Over the past several decades, empirical and theoretical research has unraveled the physics underlying edge fracture. The knowledge obtained has allowed rheologists to develop techniques to minimize the adverse effect of fracture in their experiments. In recent years, edge fracture has also been used to break up viscoelastic liquid bridges quickly and cleanly, showing its potential to be adapted to the design of functional dispensing nozzles. This Perspective article aims to give a historical overview of edge fracture and suggests research directions to develop methods for suppressing or harnessing the phenomenon to benefit applications of both fundamental and technological importance. *© 2023 Author(s). All article content, except where otherwise noted, is licensed under a Creative Commons Attribution (CC BY) license (http://creativecommons.org/licenses/by/4.0/).* https://doi.org/10.1122/8.0000625

I. INTRODUCTION

The cone-and-plate and parallel-plate fixtures are commonly used for the shear rheometry of highly viscous fluids. However, liquids such as molten polymers and particulate suspensions are rheologically complex. For instance, they can develop normal stresses in the flow when subjected to shear. When the second normal stress difference is sufficiently large, *edge fracture* can occur, causing a sudden indentation of the fluid's free surface (Fig. 1). The fracture can invade the fluid sample and decrease the contact area between the sample and the rheometer fixture, rendering rheological measurement results invalid at high-shear rates [1–9]. It can also induce apparent shear bands in the fluid bulk, making the interpretation of experimental results challenging [10].

Due to the adverse effect of edge fracture on rheometry, numerous experimental and theoretical studies have been performed over the past several decades to understand the phenomenon. The knowledge obtained has enabled rheologists to formulate strategies to suppress edge fracture. In recent years, constructive efforts have also been made to use edge fracture to destabilize viscoelastic liquid bridges quickly and cleanly [11–13]. This Perspective article aims to give an overview of edge fracture research and point out research directions that may help further suppress edge fracture or use edge fracture to benefit scientific and technological applications. The focus will be on viscoelastic fluids; however, examples with plasticity effects involved will also be

discussed. Whenever possible, theoretical and numerical predictions will be compared to empirical evidence.

II. RELEVANT DIMENSIONLESS NUMBERS

The response of a complex fluid to the shearing motion imposed by a rheometer depends on how inertia, elasticity, plasticity, and capillarity interact. Gravity is negligible as rheological experiments are typically performed at a small length scale of $O(1 \text{ mm})$. It is helpful to define the relevant dimensionless numbers to facilitate our historical overview of edge fracture research.

Considering a fluid of density ρ, zero-shear viscosity η_0, relaxation time τ, yield stress σ_y, and interfacial tension Γ subject to a characteristic shear rate of $\dot{\gamma} = U/L$, where U and L are the characteristic flow velocity and length scale, the fluid response is governed by five dimensionless numbers. With $\sigma_c = \eta_0 \dot{\gamma}$ the characteristic shear stress, the Reynolds number $\text{Re} = \rho U^2/\sigma_c$ is the ratio of inertial and viscous stresses. Assuming that the Newtonian contribution to η_0 is negligible compared to the non-Newtonian contribution, the Weissenberg number $\text{Wi} = \tau \eta_0 \dot{\gamma}^2/\sigma_c = \tau \dot{\gamma}$ is the ratio of elastic and viscous stresses. The Bingham number $\text{Bn} = \sigma_y/\sigma_c$ is the ratio of yield stress and viscous stress, and the capillary number $\text{Ca} = \sigma_c H/\Gamma = \eta_0 U/\Gamma$ is the ratio of viscous stress and the Laplace pressure. There is also the normal stress ratio $\Psi = -N_2/N_1$, where $N_1 = \sigma_{\theta\theta} - \sigma_{zz}$ and $N_2 = \sigma_{zz} - \sigma_{rr}$ are the first and second normal stress differences, and σ_{rr}, $\sigma_{\theta\theta}$, and σ_{zz} are the shear-induced radial, azimuthal, and axial normal stresses, respectively.

The Weissenberg number Wi deserves attention, as the elastic stress it characterizes is the first normal stress difference N_1 [14]. Such a definition of Wi stems from the upper-

---

a)Author to whom correspondence should be addressed; electronic mail: santo.chan@oist.jp
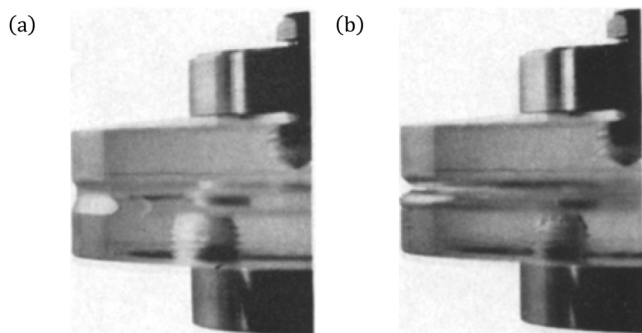
(a)   (b)

FIG. 1. Edge fracture instability of silicone oil in a cone-and-plate rheometer of cone angle 4° and plate radius 3.25 cm at a shear rate of 7.2 s^{-1}. (a) Before fracture. (b) During fracture. Reproduced with permission from Hutton, Rheol. Acta **8**(1), 54–59 (1969). Copyright 1969, Springer Nature.

FIG. 2. Shear stress response σ as a function of time t at different applied step shear rates $\dot{\gamma}$ of a silicone oil. The decrease in $\sigma(t)$ for $\dot{\gamma} = 1060$ and 1200 s^{-1} was caused by edge fracture. Reproduced with permission from Hutton, Nature **200**(4907), 646–648 (1963). Copyright 1963, Springer Nature.

convected Maxwell model proposed by Oldroyd [15]. In the context of edge fracture, a more relevant dimensionless number is the Tanner number

$$\text{Tn} \equiv 2\Psi\text{WiCa} = \frac{|N_2|L}{\Gamma}, \qquad (1)$$

which is the ratio of the second normal stress difference and the Laplace pressure. The naming of Tn was suggested by Professor Gareth H. McKinley in 2021 during the Princeton Center for Theoretical Science Workshop on Viscoelastic Flow Instabilities and Elastic Turbulence, in recognition of Professor Roger I. Tanner's contribution to the understanding of edge fracture. The current authors then used the dimensionless number in several edge fracture studies [11–13,16]. The relevance of Tn to edge fracture will become obvious in Sec. III.

III. ONSET OF EDGE FRACTURE

A. Edge fracture as a viscoelastic phenomenon

Early principal studies regarding the onset of edge fracture were done by Hutton [1–3], who photographed the phenomenon and conducted critical experiments revealing the viscoelastic nature of the instability. Using a rheometer equipped with a cone-and-plate fixture, Hutton [1] performed shear start-up experiments on a silicone oil with zero-shear viscosity $\eta_0 = 28.8$ Pa s and interfacial tension $\Gamma = 21.5$ mN m^{-1}. Step shear rates of different magnitudes $\dot{\gamma}$ were applied, and the corresponding shear stress responses σ were recorded as functions of time t (Fig. 2). For intermediate values of $\dot{\gamma}$, $\sigma(t)$ plateaued soon after the step shear rate was applied. However, when $\dot{\gamma}$ was sufficiently high, $\sigma(t)$ dropped over time. The higher the applied shear rate $\dot{\gamma}$, the sooner the drop began, and the greater the magnitude of the drop. Such a fall in $\sigma(t)$ was attributed to the conical fracture nucleated on the silicone oil's free surface, which tended to grow radially inward to the sample's bulk, decreasing the effective shearing area of the sample and hence lowering the torque measured by the rheometer. As long as the fluid sample was not expelled from the rheometer fixture, the fall in $\sigma(t)$ was observed to be recoverable. When a subsequent $\dot{\gamma}$ of intermediate magnitude was applied, $\sigma(t)$ would reach the
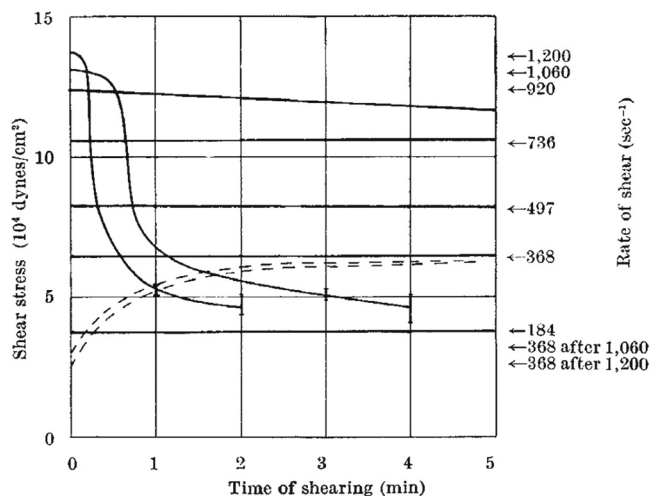
corresponding plateau value (see dashed lines in Fig. 2). This ruled out the possibility that the drop in $\sigma(t)$ and the fracture at high-shear rates were caused by the shear degradation of the silicone oil.

Hutton then tracked the temperature rise of the silicone oil during the step shear experiments, which was negligible, indicating that neither the fall in $\sigma(t)$ nor the nucleation of fracture was caused by the heating of the fluid sample. They also performed the same step shear experiments by replacing the silicone oil with Newtonian mineral oils of lower viscosity. Signatures of turbulence were not observed in the range of the shear rates tested. From this, Hutton concluded that the fracture of the silicone oil was not caused by turbulence either. One critical observation that Hutton made was that the silicone oil tended to climb up the rotating part of the cone-and-plate fixture when the fracture occurred, resembling the rod-climbing phenomenon reported by Weissenberg [17]. This implied that the silicone oil was viscoelastic, leading to the author's supposition that the fracture was an elastic effect.

Postulating that fracture would occur when the elastic energy is sufficient to supply energy for creating new surfaces, Hutton derived the following criterion for the fracture phenomenon to occur:

$$N_1 > k\frac{\Gamma}{H}, \qquad (2)$$

with N_1 the first normal stress difference and k a numerical constant related to the fraction of elastic energy converted into surface energy. For the parallel-plate fixture, H refers to the gap size. For the cone-and-plate fixture, $H = R_p\phi$, where R_p and ϕ are the plate radius and cone angle, respectively. Experiments using silicone oils of different zero-shear viscosity and cone-and-plate fixtures of different $R_p\phi$ were performed, which verified the relation regarding the critical first normal stress difference $N_{1c} \propto 1/R_p\phi$ predicted in Eq. (2).

The same fracture phenomenon was observed in a parallel-plate fixture in a subsequent study [3]. Since theory predicted that secondary flows due to elastic forces could not occur in a parallel-plate fixture of infinite radius, the possibility of them causing fracture was low, suggesting that the fracture was an interfacial instability rather than a bulk instability, hence the name edge fracture. Incidentally, Hutton [2] also attempted to employ their criterion of edge fracture to explain melt fracture, the surface distortions typically observed in molten polymers extruding through a capillary at high-shear rates [18], by assuming that the phenomenon was caused by the cohesive failure within the polymer bulk. Several scholars [19,20] later adapted Hutton's idea in developing their models for melt fracture.

B. The Tanner–Keentok criterion

The criterion proposed by Hutton [1–3] offered an essential insight that edge fracture is an elastic phenomenon. However, it was deduced based on energy arguments. The first normal stress difference N_1 was believed to be responsible for nucleating the fracture simply because its magnitude for most viscoelastic fluids was more significant than the second normal stress difference N_2. This assumption was later questioned by Tanner and Keentok [4], who derived their criterion of edge fracture based on fracture mechanics principles.

Tanner and Keentok [4] considered the steady shear flow of a second-order fluid in a parallel plate fixture with a plate radius R_p much larger than the gap size H, approximating the planar Couette geometry. A preexisting semicircular crack of diameter $2a \ll H$ was assumed on the free surface of the fluid sample. Imposing the no-penetration and zero-shear stress boundary conditions on the free surface and balancing the maximum radial normal stress to the Laplace pressure on the crack, Tanner and Keentok derived their criterion for edge fracture

$$|N_2| > \frac{2\Gamma}{3a}.\tag{3}$$

When the criterion is satisfied, the second normal stress difference N_2 will deepen the crack; otherwise, the Laplace pressure Γ/a will close the crack. The criterion can alternatively be expressed in terms of the Tanner number [Eq. (1)] as

$$\mathrm{Tn} = \frac{|N_2|}{\Gamma}2a > \frac{4}{3}.\tag{4}$$

The first normal stress difference N_1 is not involved as it was canceled out during the derivation of Eq. (3). However, one must note that N_1 could affect the propagation dynamics of the fracture, which Tanner and Keentok did not consider in their model.

Using a rheometer equipped with a cone-and-plate or a parallel-plate fixture, Tanner and Keentok then characterized different fluids' normal stress and edge fracture behaviors. The measured critical second normal stress differences N_{2c}

seemed to agree with Eq. (3). However, when calculating the right-hand side of the criterion, the authors assumed the same crack size of a for all fluid samples tested. This was a critical assumption, as the value of a was obtained from a single measurement of silicone oil with a zero-shear viscosity $\eta_0 = 10.6\,\mathrm{Pa\,s}$, zero-shear second normal stress coefficient $\Psi_{2,0} \equiv N_2/\dot{\gamma}^2 = 5\,\mathrm{mPa\,s}^{-2}$, and interfacial tension $\Gamma = 20.3\,\mathrm{mN\,m}^{-1}$ at a specific shear rate.

The Hutton and the Tanner–Keentok criteria could be obtained using dimensional analysis arguments [4]. They only differ in their assumptions regarding the governing normal stress difference. Hutton assumed that the first normal stress difference N_1 was responsible for edge fracture, while Tanner and Keentok argued that it was the second normal stress difference N_2. Lee et al. [5] performed a critical study disproving the Hutton criterion. They considered six polymer solutions with normal stress ratio $0 \leq \Psi \leq 0.3$, where $\Psi = -N_2/N_1$ and roughly, the same interfacial tension $\Gamma = 30\,\mathrm{mN\,m}^{-1}$. A cone-and-plate fixture flush-mounted with four miniature pressure transducers was used to measure the critical normal stress differences N_{1c} and N_{2c} at which edge fracture occurred (Fig. 3). N_{1c} varied almost an order of magnitude among the five fluid samples with $\Psi > 0$ that underwent fracture. For the sample with $\Psi = 0$, edge fracture was not observed within the shear rate range tested. These two pieces of evidence offered counterexamples to the Hutton criterion. In contrast, the magnitudes of N_{2c} were almost the same, supporting the Tanner–Keentok criterion.

Subsequently, Huilgol et al. [6] reexamined the planar Couette flow of a second-order fluid considered by Tanner and Keentok [4]. Assuming that the velocity field is azimuthal, they showed that the zero-shear stress boundary

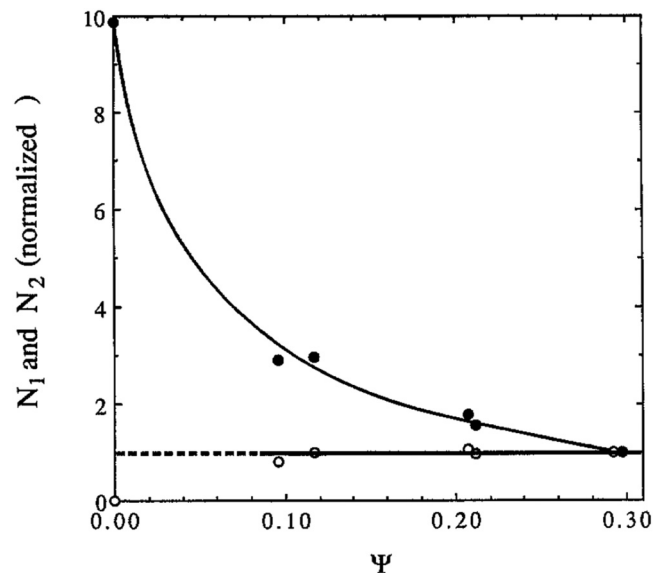**FIG. 3.** Critical first and second normal stress differences N_{1c} (filled symbols) and N_{2c} (empty symbols) of edge fracture as a function of the normal stress ratio $\Psi = -N_2/N_1$. N_{1c} and N_{2c} were normalized by the values observed for the fluid sample having the largest Ψ. Reproduced with permission from Lee et al., Rheol. Acta **31**(3), 306–308 (1992). Copyright 1992, Springer Nature.

condition on the fluid's free surface would require that

$$\Psi_2(\nabla w \cdot \mathbf{n})(\mathbf{n} \times \nabla w) = \mathbf{0}, \qquad (5)$$

where w is the azimuthal velocity component and $\mathbf{n}$ is the unit normal vector to the fluid's free surface. The flow that Tanner and Keentok considered satisfied the above condition as the no-penetration boundary condition $\nabla w \cdot \mathbf{n} = 0$ was assumed in the derivation of their edge fracture criterion. Huilgol *et al.* also showed that the radial normal stress acting on the semicircular crack assumed by Tanner and Keentok was indeed tensile. The authors further noted that Eq. (5) could also be satisfied by demanding that the surface normal be parallel to the velocity gradient, i.e., $\mathbf{n} \times \nabla w = \mathbf{0}$. Such a condition was claimed to be possible after the fracture had penetrated the fluid sample, with its free surface taking on a profile nearly parallel to the fixture plates. In such a case, the normal stress would tend to compress the fracture surface, closing the crack and stopping its propagation.

The theoretical prediction of Huilgol *et al.* regarding the normal stress distributions around the fracture surface was later tested by Keentok and Xue [7]. The authors simulated the planar Couette flow using the Phan-Thien–Tanner model [21]. A rectangular crack of fixed width and depth was assumed on the liquid-air interface, located symmetrically halfway between the plates. The no-slip boundary condition was imposed on the parallel plates, while the no-penetration and zero-shear stress boundary conditions were imposed on the liquid-air interface. The finite volume method was employed to obtain the numerical solutions for the velocity and stress fields. Although the meniscus of the fluid was not modeled as a free surface, the simulated normal stress distributions around the fracture agreed with the analysis of Huilgol *et al.* [6]

Keentok and Xue also experimentally investigated the edge fracture behavior of a wide range of fluids, including three silicone oils, two Boger fluids, a lubricating grease, and a toothpaste. The authors made several important observations. First, the Boger fluids with second normal stress coefficients $\Psi_2 \approx 0$ did not undergo edge fracture, agreeing with the Tanner–Keentok criterion [4]. Second, the diameter a of the semicircular crack increased when the gap size H of the rheometer fixture was increased; however, a/H was not a constant but inversely proportional to H. Third, the ratio $3aN_{2c}/2\Gamma$ appeared to increase with the Reynolds number $\mathrm{Re} = \rho R_p^2 \Omega/\eta_0$, where Ω is the rotational speed of the rheometer cone or plate, suggesting that inertia tends to oppose edge fracture. As a side note, the authors indicated that measuring N_1 and N_2 of the lubricating grease was difficult. Potentially, the problem was caused by the finite yield stress in the fluid, which could shift the normal stress signal baseline and thus interfere with the measurement [22].

C. Edge fracture and shear banding

Intense shearing can often induce localized velocity bands of different shear rates, aka shear bands, in a rheologically complex fluid [23–30]. Its underlying physics has been constantly debated, especially for entangled polymers where artifacts such as wall slip and edge fracture can affect the interpretation of experimental results [10,31–44]. It has also been shown that flow-induced nonuniformity of the polymer concentration is related to shear banding [45–51]. The literature regarding shear banding is vast; interested readers are referred to the excellent reviews written by Wang [29] and Germann [30]. The current article will focus only on studies where shear banding was deemed essential to developing edge fracture and vice versa.

Using an entangled 10 wt. % polybutadiene in oligomeric butadiene solution with roughly 47 entanglements per chain, Tapadia and Wang [31,32] observed a discontinuity in the flow curve when performing rheological experiments in the cone-and-plate, parallel plate, and concentric cylinder fixtures. The small amplitude oscillatory shear (SAOS) test result showed a typical shear thinning behavior. However, as the shear stress varied across a critical value in the controlled stress flow sweep experiment, the apparent steady-state shear rate jumped discontinuously, spanning two to three decades of shear rates. As the shear rate varied in a controlled-rate flow sweep, the shear stress seemed to plateau over two to three decades of shear rates, corresponding to the discontinuous jump. The authors interpreted their observations as the consequence of an entanglement-disentanglement transition of the polymer molecules, similar to the solid-liquid transition of a yield stress fluid.

In a subsequent study, Inn *et al.* [33] repeated Tapadia and Wang's experiments and obtained a similar flow curve using the same polymer solution and an additional 7.5 wt. % solution. However, they noticed that edge fracture occurred when the shear stress was increased in the controlled stress flow sweep experiment. Hence, the entanglement-disentanglement transition that Tapadia and Wang proposed might be an experimental artifact caused by the fracture. The disagreement between the two interpretations ignited several works concerning whether the flow curve of the entangled polymer solution is monotonic. In some of those works, edge fracture in the concentric cylinder fixture was reported (e.g., Fig. 4), and new ideas to mitigate edge fracture were proposed [34–52]. Those mitigation methods will be the focus of Sec. IV. As a side note, Inn *et al.* also observed that if the flow sweep experiment was conducted in reverse, where sufficiently high applied shear stress was first applied and gradually decreased, edge fracture appeared less severe. The effect of fracture became more pronounced when the applied shear stress was reduced. Such a stabilizing effect remains unexplained; it may be due to the fluid sample's wall slip typically observed for entangled polymers subjected to high-shear stress [26,29], which tends to suppress edge fracture [53].

The possibility that edge fracture can lead to apparent shear banding has major implications for rheologists. As a result, research has also been carried out to uncover the effect of edge disturbance on rheological measurements. For instance, Schweizer and Stöckli performed simultaneous shear start-up tests and particle tracking velocimetry on a monodisperse and a polydisperse polystyrene melt. A total of 21 pretreatment protocols were considered, which involved cone-and-plate fixtures of two different cone angles ϕ,
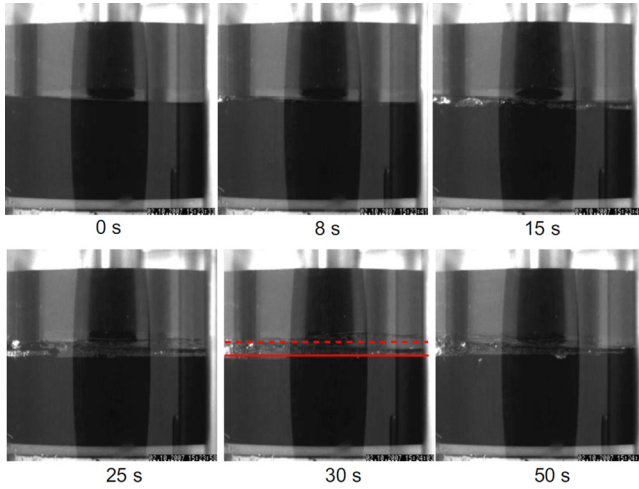
FIG. 4. Development of edge fracture in polybutadiene in oligomeric butadiene solution subjected to a constant torque of 200 mN for 15 s followed by a shear rate of $5\,\mathrm{s}^{-1}$ for 85 s in a concentric cylinder fixture. Edge fracture can be seen at 15 s, causing the apparent sample height to decrease as time proceeds. The broken red line at 30 s represents the initial sample height; the solid red line represents the apparent sample height after the occurrence of edge fracture. Reproduced with the permission from Hu, J. Rheol. **54**(6), 1307–1323 (2010). Copyright 2010, AIP Publishing LLC.

FIG. 5. The effect of the (a) ideal, (b) convex, and (c) concave edge profiles on the fluid sample's surface velocity profile in a cone and plate rheometer fixture at different times t. Reproduced with the permission from Schweizer and Stöckli, J. Rheol. **52**(3), 713–727 (2008). Copyright 2008, AIP Publishing LLC.

different loading gap sizes for the polymer melt sample, different temperatures and duration for conditioning the sample's edge, and different temperatures and duration for equilibrating the sample. Those protocols allowed samples with different initial edge profiles to be prepared. The authors categorized the edge profiles into ideal, convex, and concave. For an ideal edge, the polymer melt completely wets the rheometer plate. The sample wetting radius r_w and the surface radius of curvature r_c equal the plate radius R_p; the sample surface is part of a sphere centered on the cone-and-plate fixture's rotation axis. In such a case, the authors observed that the azimuthal flow velocity v_x measured on the sample's surface varies linearly to the y axis, i.e., dv_x/dy is a constant, agreeing with the theoretically predicted velocity profile for the cone-and-plate fixture [Fig. 5(a)]. For a convex edge, r_c is positive and smaller than R_p. The measured velocity profile on most parts of the sample's surface was linear, with the shear rate being lower than the theoretical prediction, except close to the cone and the plate, where two high-shear rate layers were observed [Fig. 5(b)]. For a concave edge, r_c is negative. The measured velocity profile was nonlinear, with a high-shear rate layer in the sample's vertical midplane [Fig. 5(c)]. The authors speculated that the nonideal convex and concave edges could lead to an inhomogeneous distribution of the second normal stress difference N_2, which could amplify the curvature of the sample's surface, leading to edge fracture, in turn making the velocity profile even more nonlinear and forming the experimentally observed high-shear rate layers.

D. The Skorski–Olmsted criterion

Aiming to clarify the relation between shear banding and edge fracture, Skorski and Olmsted [39] analyzed how shear banding could induce fracture in a planar Couette geometry.
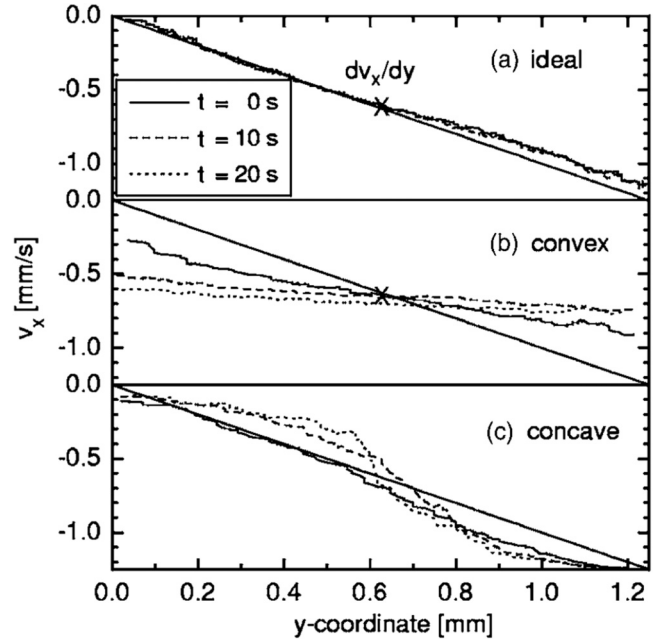
They considered the force balance, continuity, and smoothness of the fluid's free surface. With $\langle\dot{\gamma}\rangle$ being the applied average shear rate, $\dot{\gamma}_1, \dot{\gamma}_2$ being the lower and upper shear rate values delimiting the shear stress plateau in the flow curve, ψ being the contact angle on each plate of the geometry, $\Delta N_2 < 0$ being the difference in the second normal stress differences across the two shear bands, Γ being the interfacial tension, and H being the geometry gap size, the dimensionless radii of curvature $\hat{R}_1$ and $\hat{R}_2$ of the two free fluid surfaces enclosing the shear bands are

$$\hat{R}_1 = \frac{1}{-2\cos\psi - \hat{w}_2 A}, \tag{6}$$

$$\hat{R}_2 = \frac{1}{-2\cos\psi + \hat{w}_1 A}, \tag{7}$$

where $\hat{w}_1 = (\dot{\gamma}_2 - \langle\dot{\gamma}\rangle)/(\dot{\gamma}_2 - \dot{\gamma}_1)$ and $\hat{w}_2 = (\langle\dot{\gamma}\rangle - \dot{\gamma}_1)/(\dot{\gamma}_2 - \dot{\gamma}_1)$ are the normalized shear bandwidths and $A = -H|\Delta N_2|/\Gamma$ is the so-called distortion parameter. By requiring the two free fluid surfaces not to have an infinite slope or pass through each other, Skorski and Olmsted derived the surface integrity conditions

$$|(\hat{w}_2 - \hat{w}_1)\cos\psi - \hat{w}_2 A| < 1, \tag{8}$$

$$-1 - \cos\psi < \frac{\hat{w}_i}{\hat{R}_i} < 1 - \cos\psi. \tag{9}$$

The contact angle ψ is defined by the interfacial properties of the fluid and fixture plates. For a given flow curve showing

shear banding, the shear bandwidths $\hat{w}_1$ and $\hat{w}_2$ are uniquely determined by $\langle\dot{\gamma}\rangle$. Hence, whether the surface of a fluid subjected to a specific shear rate satisfies Eqs. (8) and (9) is solely determined by the distortion parameter A. For $-2 < A < 0$, the integrity conditions are satisfied for all ψ. For $A < -2$, the conditions are violated by some ψ. While for $A < -4$, the conditions are violated for all ψ. By fitting the Johnson–Segalman [54] and Giesekus [55,56] constitutive models to flow curves of wormlike micellar solutions [57,58] and entangled polymer solutions [36] showing shear banding, the authors showed that the surface integrity criterion $A < -2$ could predict the onset of edge fracture in those experiments reasonably well. In terms of the Tanner number [Eq. (1)], the criterion can be restated as

$$\text{Tn} = \frac{|\Delta N_2|}{\Gamma} H > 2, \tag{10}$$

which assumes the same form and the same order of magnitude $O(1)$ as Eq. (4), showing the similarity of the fracture caused by shear banding to that caused by simple shear as studied by Tanner and Keentok [4].

E. The Hemingway–Fielding criterion

The Tanner–Keentok and Skorski–Olmsted models could explain the roles of the second normal stress difference and the Laplace pressure in inducing edge fracture. However, they have multiple weaknesses in a theoretical sense. First, the two models were derived from the static force balance across the fluid's free surface, whereas edge fracture is a dynamic process. Second, the Tanner–Keentok model assumed a preexisting semicircular crack of diameter a, which lacked a physical explanation [4]. Third, the Skorski–Olmsted model only showed that shear banding could induce fracture; whether fracture can cause apparent shear banding in the fluid remained unclear [39].

To resolve these problems, Hemingway and Fielding [8] performed linear stability analysis on the planar Couette flow using the Johnson–Segalman and Giesekus models. In the limit of low Weissenberg number $\text{Wi} = \tau\dot{\gamma} \ll 1$ where both models reduce to the second-order model, the authors derived that

$$\frac{1}{2}\Delta\sigma \frac{d|N_2(\dot{\gamma})|}{d\dot{\gamma}} \Big/ \frac{d\sigma}{d\dot{\gamma}} > \frac{2\pi\Gamma}{H}, \tag{11}$$

which provided an essential insight that the jump in the shear stress $\Delta\sigma$ between the fluid and the outside medium may also contribute to the development of edge fracture. For the second-order model, $N_2 = \Psi_2\dot{\gamma}^2$, where the second normal stress coefficient Ψ_2 is a constant. Further assuming that the medium surrounding the fluid sample is air, which has a viscosity negligible compared to the fluid viscosity, gives $\Delta\sigma = \sigma = \eta_0\dot{\gamma}$. In such a case, the Hemingway–Fielding criterion [Eq. (11)] reduces to the Tanner–Keentok criterion [Eq. (3)] as

$$|N_2| > \frac{2\pi\Gamma}{H}, \tag{12}$$

with the dominant wavelength of the free surface instability $H/2\pi$ replacing the crack radius a assumed by Tanner and Keentok. In terms of the Tanner number [Eq. (1)], the criterion can be written as

$$\text{Tn} = \frac{|N_2|}{\Gamma} \frac{H}{2\pi} > 1. \tag{13}$$

Phase-field simulations of the planar Couette flow by the same authors using the Johnson–Segalman and Giesekus models showed that Eq. (11) could predict the onset of edge fracture for $\text{Wi} < 1$ [8]; a state diagram and the corresponding snapshots of the phase-field simulation predicted by the Giesekus model are shown in Fig. 6. Nonetheless, the predictions are yet to be experimentally verified.

To study the interplay between edge fracture and shear banding, Hemingway and Fielding [10] then simulated the planar Couette flow of fluids having either a monotonic or
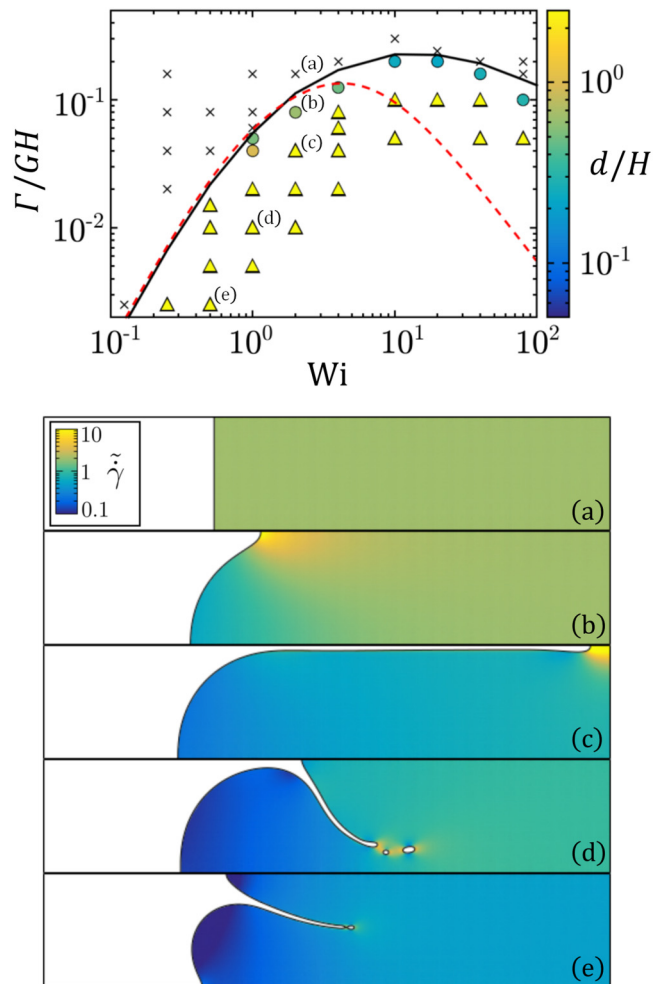

FIG. 6. Simulated state diagram of a Giesekus fluid sheared in a planar Couette flow geometry in the space of dimensionless surface tension Γ/GH and Weissenberg number Wi. d is the edge fracture's penetration depth into the fluid sample. Black solid line: numerically measured edge fracture threshold. Red dashed line: prediction of the Hemingway–Fielding criterion [Eq. (11)]. (a)–(e) Snapshots of the phase-field simulation corresponding to the state points labeled in the state diagram. $\tilde{\dot{\gamma}}$ is the frame invariant shear rate. Reproduced with the permission from Hemingway and Fielding, J. Rheol. **63**(5), 735–750 (2019). Copyright 2019, AIP Publishing LLC.

nonmonotonic flow curve by varying the material parameters of the Johnson–Segalman and Giesekus models. For fluids with a monotonic flow curve, slight disturbances on their free surface were found to cause an apparent shear banding in the fluid bulk [e.g., Fig. 6(b)]. For a fixed interfacial tension value, the degree of edge disturbance and apparent shear banding increased as the fluid was set to be more shear-thinning. Increasing the interfacial tension could suppress the occurrence of apparent shear banding. For fluids having a nonmonotonic flow curve, in the shear rate regime where the bulk flow was not shear banded, the interface remained undisturbed if the interfacial tension was sufficiently high; otherwise, it was constantly disturbed. The authors also compared the ability of the Hemingway–Fielding [Eq. (11)] and Skorski–Olmsted [Eqs. (8) and (9)] criteria to predict the simulated onset of edge fracture due to shear banding. While the former could predict the fracture onset reasonably well, the latter over-predicted it. Hemingway and Fielding attributed such a disagreement to the presence of secondary flows near the fluid's free surface, which broke down the assumptions made by Skorski and Olmsted [39]. However, it is crucial to recall that during the derivation of the Hemingway–Fielding criterion [Eq. (11)], $\text{Wi} \ll 1$ was assumed [8]. Hence, the agreement between the criterion and the simulated edge fracture onset at high-shear rates with $\text{Wi} > 1$ was likely coincidental. The authors also stressed this point in their discussion. The findings of Hemingway and Fielding are of fundamental importance to the research of shear banding; they enforced the view that edge effects must be eliminated if one desires to study the phenomenon experimentally.

F. The Tanner number Tn

The Tanner–Keentok criterion was constructed to predict edge fracture for second-order fluids [4]. On the other hand, the Skorski–Olmsted criterion was proposed for shear banding fluids [39]. The Hemingway–Fielding criterion unified the two criteria as it was constructed based on the Johnson–Segalman and Giesekus models, which reduce to the second-order model for $\text{Wi} \ll O(1)$ and show shear banding behavior for $\text{Wi} \in O(1)$ if suitable material parameters are chosen [8,10].

Expressing the edge fracture criteria in terms of the Tanner number [Eq. (1)] resulted in Eqs. (4), (10), and (13), which all satisfy the condition $\text{Tn} \gtrsim 1$. Hence, the edge fracture criterion can be generalized as follows:

$$\text{Tn} = \frac{|N_2|L}{\Gamma} \geq O(1), \tag{14}$$

with L being the characteristic length scale of the flow of interest. The second normal stress difference will dominate for $\text{Tn} \geq O(1)$; edge fracture will likely occur. Otherwise, the Laplace pressure will stabilize the fluid's free surface. For two reasons, we argue that Tn is more suitable than Wi in the context of edge fracture. First, Tn is defined based on the theory of fracture; it describes more accurately the relevant stresses than Wi. Second, Tn has a more well-defined critical value of $O(1)$ to predict fracture than Wi; for instance, edge fracture is predicted for $\text{Wi} \ll O(1)$ in the Tanner–Keentok and Hemingway–Fielding models and $\text{Wi} \in O(1)$ in the Skorski–Olmsted model.

IV. MITIGATION OF EDGE FRACTURE

Because of its adverse effects on rheometry, different strategies have been employed over the past several decades to mitigate edge fracture. Some prominent examples will be discussed in this section.

A. Strategies based on edge fracture criteria

The Hemingway–Fielding criterion states that the Laplace pressure tends to oppose the action of the second normal stress difference. Hence, the simplest way to delay the onset of edge fracture is to decrease the gap size H of the parallel-plate fixture (or $R_p\phi$ of the cone-and-plate fixture). Hutton's experimental results [1–3] verified the applicability of this method. However, one must be cautious that the technique may lead to incorrect rheological measurement results if H is too small, as the gap error due to nonparallelism and zeroing procedure of the parallel plates will become increasingly important; calibration procedures have to be employed to correct for the gap error [59–62]. On the other hand, for the cone-and-plate fixture, a small cone angle ϕ can lead to wrong normal stress measurement results, as the shear-induced first normal stress difference N_1 tends to push the cone and plate apart, introducing a squeeze flow with a relaxation time scale $\tau_s = 6\pi R_p \eta_0 / K_A \phi^3$, where K_A is the rheometer's axial stiffness [63].

The Laplace pressure can also be increased by sealing the fluid sample's free surface with a sealant such that the sample-sealant interface has a higher interfacial tension. In their study of the rheology of hydroxypropyl cellulose liquid crystalline aqueous solution, Grizzuti et al. [64,65] used mercury, a liquid metal, as the sealant to prevent their fluid sample from evaporating. They observed that edge fracture could be delayed for around two decades of shear rate, so they had to stop their measurement due to the stress transducer overload. Keentok and Xue [7] later explained Grizzuti et al.'s observation using the Tanner–Keentok criterion. However, even though using mercury as the sample sealant could delay edge fracture, the method did not receive much attention from the rheology community. This is likely due to the toxicity of mercury as it evaporates [66].

To solve the toxicity problem, in their recent study, Chan et al. [16] replaced the mercury with the nontoxic liquid metal galinstan, a eutectic alloy composed of gallium, indium, and tin [67], a material commonly used by computer enthusiasts to cool down their hardware. Using a well-characterized silicone oil with interfacial tensions of $\Gamma_a = 20.6\,\text{mN}\,\text{m}^{-1}$ and $\Gamma_g = 496\,\text{mN}\,\text{m}^{-1}$ with air and galinstan, respectively, the authors showed that sealing the fluid sample with galinstan can delay fracture occurrence by a decade of shear rate compared to the conventional cone-and-plate fixture. This makes it a promising method for preventing, rather than simply suppressing, the adverse effects of edge fracture.

B. Guard ring assembly

Removing the fluid sample's free surface from the rheometer rim can also delay edge fracture. To characterize the shear and normal stress behaviors of a set of viscoelastic suspensions made of silicone oils and glass microbeads, Mall-Gleissle *et al.* [68] installed a guard ring assembly onto the cone-and-plate fixture. The guard ring (designed by Gleissle [69]) created a well containing the fluid sample, which eliminated the sample's free surface from the fixture's rim, extending the measuring shear rate range by approximately two to three times without affecting the normal stress measurement. However, a correction procedure for the shear stress measurement was necessary to compensate for the extra torque from the excess fluid sample between the shearing gap and the guard ring. This involved vertically shifting the flow curve obtained with the guard ring to match that obtained without.

Pieper and Schmid [70] later investigated how using guard rings may affect the flow field in a parallel-plate fixture for different fluid samples, including a Newtonian fluid (mixture of polyethylene glycol, a sodium iodine aqueous solution, and the nonionic surfactant Triton-X100), a set of suspensions made of the Newtonian fluid and polymethyl methacrylate microparticles, and a strongly shear-thinning Xanthan gum solution. Particle image velocimetry showed that the existence of the guard ring would cause the parallel-plate flow to deviate from the theoretical prediction. The deviation was observed to be more severe as the fluid sample became more shear-thinning. Hence, the shear rate can be challenging to define in the presence of a guard ring, especially when the fluid has a non-Newtonian viscosity. As the guard ring violates the boundary condition for simple viscometric flows, it should be avoided whenever possible.

C. Cone-partitioned plate fixture

Another method to mitigate edge fracture is the cone-partitioned plate (CPP) fixture, a modification of the cone-and-plate fixture in which the plate is divided into two portions: an inner disk of radius R_i that is coupled to the stress transducer and an outer ring of radius R_o that is mounted to the rheometer frame. An in-depth analysis and historical overview of the fixture is beyond the scope of the current article; interested readers are referred to the excellent articles written by Vlassopoulos and coworkers [71,72]. In what follows, we will briefly mention the history of the CPP fixture, focus on studies that are deemed closely related to edge fracture and discuss some limitations of the fixture and the ways around them.

The fixture was originally designed by Meissner *et al.* [73] to measure the normal stress differences N_1 and N_2 of a low-density polyethylene melt but not to suppress the adverse effect of edge fracture. The radial distribution of the axial normal stress across the plate was shown to be

$$\sigma_{zz}(r) = \sigma_{zz}(R_s) + (N_1 + 2N_2)\ln\frac{r}{R_s}, \qquad (15)$$

with r being the radial distance from the plate's center and $R_i \leq R_s \leq R_o$ being the radius of the fluid sample.

Integrating $2\pi r\sigma_{zz}(r)$ from $r = 0$ to R_s gave the total normal force exerted by the sample

$$F_s = \frac{\pi}{2}R_s^2 N_1. \qquad (16)$$

Meanwhile, integrating $2\pi r\sigma_{zz}(r)$ from $r = 0$ to R_i gave the relation

$$\frac{F_i R_s^2}{F_s R_i^2} = 1 + 2\left(1 + \frac{2N_2}{N_1}\right)\ln\frac{R_s}{R_i}, \qquad (17)$$

where F_i is the normal force acting on the inner disk. Since R_s and R_i were both known quantities, by measuring N_1 using a conventional cone-and-plate fixture and Eq. (16), the authors were able to measure N_2 using the cone-and-partitioned plate fixture and Eq. (17).

Realizing the accessory's potential in mitigating the adverse effects of edge fracture, Schweizer [74–76] conducted experiments to compare the conventional cone-and-plate fixture and the CPP fixture having the same cone angle. The author first applied a step shear rate of different magnitudes $\dot{\gamma}$ to a polystyrene melt and recorded the start-up viscosity $\eta \equiv \sigma/\dot{\gamma}$ over time t, where σ is the shear stress response. For the cone-and-plate fixture, at a sufficiently high-shear rate, $\eta(t)$ decreased over time due to the penetration of edge fracture into the fluid sample. However, for the CPP fixture, $\eta(t)$ could reach a steady state before dropping in magnitude, as long as R_s was sufficiently bigger than R_i. This signified that the time needed for the flow to become steady was shorter than that for the fracture to propagate to the central measurement area of the partitioned plate. Plotting the steady-state value of $\eta(t)$ versus $\dot{\gamma}$ allowed Schweizer to extend the shear rate range of the flow curve to around three times; the upper limit was not given by edge fracture, but the stress transducer overload at high-shear rates. The flow curve obtained using the CPP fixture was validated by the lower shear rate data obtained by the conventional cone-and-plate fixture and the even higher shear rate data obtained by a capillary rheometer.

Despite the controversial interpretation of the results, the CPP fixture had also been employed to study the shear banding of entangled polymers [37,42–44]. To characterize the shear rheology of a set of polybutadiene in oligomeric butadiene solutions, Wang and Ravindranath [37,43] attempted to eliminate edge effects by wrapping a plastic film around the outer ring of the partitioned plate, which stayed stationary regardless of the cone rotation. The authors claimed that the cone-partitioned plate fixture and the wrapped plastic film could effectively eliminate the free surface of the fluid sample, hence preventing the occurrence of edge fracture. However, Li *et al.* [42,44] later criticized the film wrapping method and performed particle tracking velocimetry [77] on a similar set of polymer solutions sheared by a parallel-plate fixture. They showed that surrounding the rim of the plates with a plastic ring could initiate apparent shear banding at a lower Wi. For instance, the shear banding was observed at Wi = 5 when the fluid

sample was sheared in a conventional parallel-plate fixture but at a lower value of Wi = 2.8 when the plastic ring was installed. The authors provided an ad hoc explanation for their observation: surrounding the fluid's free surface with the plastic ring might have changed the nature of the edge fracture but not eliminated it. This can be further illustrated by the Tanner number Tn. For the parallel-plate flow without installation of the plastic ring, the characteristic velocity U and length scale L is the rim velocity U_{rim} and the fixture gap size H, respectively. Installing the plastic ring will introduce a new length scale: the clearance $h < H$ between the ring and the plate. Recall from Eq. (1) that

$$\text{Tn} = 2\Psi \frac{\tau U}{L} \frac{\eta_0 U}{\Gamma} \propto \frac{1}{L}. \tag{18}$$

The existence of the plastic ring will, in effect, increase the characteristic Tanner number of the parallel-plate flow by a factor of H/h, given that U_{rim} is fixed. This could explain why Li et al. [42] observed shear banding at a lower Wi when the plastic ring was installed as they defined Wi based on their gap size $H \in O(1 \text{ mm})$ and ignored the potentially more relevant clearance $h \in O(0.1 \text{ mm})$. Hence, somewhat counterintuitively, covering the fluid's free surface in a rheometer fixture without completely sealing it may render edge fracture more likely to occur. Nonetheless, this supposition is yet to be tested by experiments.

The CPP fixture, despite being a powerful tool, can only mitigate the negative effects of edge fracture but cannot prevent its occurrence. Attempting to circumvent such a problem, Li and Wang [78] modified the partitioned plate to include a conical outer ring. This way, the sample edge has a height of $H > R_i\phi$. When a strain γ is applied to the fluid sample in the inner measurement region, the sample edge will experience a strain of smaller magnitude $(R_i\phi/H)\gamma$. By monitoring the motion of the tracking particles and aluminum oxide powder on the sample edge, the authors showed that using such a fixture design could eliminate edge effects in step strain and large amplitude oscillatory shear experiments. Nonetheless, it is unclear if the fixture design can also eliminate edge effects in shear start-up experiments.

Another problem of the CPP fixture is related to the measurement of N_2, whose error increases significantly as R_s is close to R_i. To overcome this problem, Schweizer and Schmidheiny [79] developed a CPP fixture with three partitions, abbreviated as the CPP3 fixture. The fixture's partitioned plate consists of three portions: an inner disk of radius R_i, a middle ring of radius R_{o1} surrounding the inner disk, and an even larger outer ring of radius R_{o2} surrounding both the inner disk and the middle ring. The inner disk and the middle ring can measure normal force signals separately, allowing Eqs. (16) and (17) to be used to measure N_1 and N_2 without having to perform experiments using a conventional cone-and-plate fixture. Meanwhile, the outer ring serves the purpose of shielding edge fracture off. Despite its great potential in measuring normal stresses, the authors stressed that the CPP3 fixture is not ideal for measuring viscosity as the torque measurement is performed solely by the rather small inner disk.

Finally, it is essential to note that the CPP fixture was designed primarily for polymer melts having a zero-shear viscosity $\eta_0 \geq O(1000 \text{ Pa s})$. Caution has to be paid when fluid samples of lower viscosity are used; the shear-induced normal stress may push the fluid into the thin gap between the partitioned plate's inner disk and outer ring, affecting the normal stress measurement. In such a case, preshearing the sample and zeroing the normal stress transducer before an experiment will be necessary. Another problem is that when the temperature is controlled with a convection oven, it becomes difficult at elevated temperatures to maintain both the inner disk and the outer ring of the partitioned plate at the same temperature. Installing an electric heating unit will be necessary for such a case [79].

V. EDGE FRACTURE OF LIQUID BRIDGES

In their landmark paper over half a century ago, Hutton wrote, "It is expected that the fracture phenomenon will be important in a number of other applications of fundamental and technological importance, but its occurrence will depend on the geometry of the device in which the liquid is sheared." [1] Nonetheless, most research on edge fracture was performed in the standard cone-and-plate and parallel-plate fixtures, focusing on mitigating the phenomenon in rheometry rather than harnessing it for practical applications. So far, only three studies have considered edge fracture in a non-rheometry setting and proposed harnessing the phenomenon to help dispense rheologically complex fluids efficiently.

Rheologically complex fluids can store energy elastically. Because of this, when such fluids are dispensed, stable liquid bridges can form between the dispensing nozzle and the substrate. Lifting the nozzle is a common way to destabilize those liquid bridges. However, as the dispensing distance increases, the liquid bridge's length also increases. In such a case, the pinchoff of the liquid bridge leads to a long capillary tail forming, which may fall randomly onto and contaminate the substrate. This is known as the stringing problem. To solve the stringing problem, Chan et al. [11,12] proposed using torsion instead of an extension to destabilize liquid bridges. To model a dispenser, they constructed a simple setup consisting of a pair of parallel plates of radius $R_p = 3 \text{ mm}$, one of which could translate vertically to set the liquid bridge height H and another that could rotate unidirectionally at angular speed Ω to apply torsion to the liquid bridge. The fixed liquid bridge volume V was controlled via a positive displacement pipet or trimming of the excess fluid at a small H. Using the setup, the authors studied how torsion could destabilize liquid bridges made of a wide range of fluids with different rheological complexity levels.

A. Weakly viscoelastic liquid bridges

Chan et al. [11] first considered liquid bridges made of weakly viscoelastic silicone oils. The focus was on a silicone oil of interfacial tension $\Gamma = 20.6 \text{ mN m}^{-1}$, similar to the fluids used in the early studies of edge fracture by Hutton [1–3] and Tanner and Keentok [4]. Its rheology could be fitted with the three-mode Giesekus model [55,56], which gave a zero-shear viscosity $\eta_0 = 58.6 \text{ Pa s}$, relaxation time
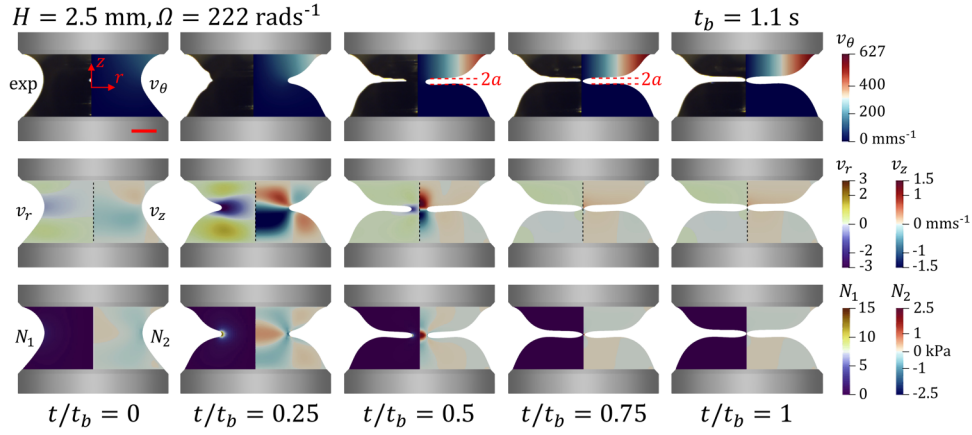
FIG. 7. Edge fracture of a weakly elastic liquid bridge made of silicone oil under an applied rotational speed of $\Omega = 222$ rad s^{-1}. Top row: experimental snapshots (left) and simulated azimuthal velocity v_θ (right). Middle row: simulated radial and axial velocities v_r (left) and v_z (right). Bottom row: simulated first and second normal stress differences N_1 (left) and N_2 (right). Scale bar: 1 mm. Reproduced with permission from Chan *et al.*, Proc. Natl. Acad. Sci. U.S.A. **118**(24), e2104790118 (2021). 2021 Author(s), licensed under a Creative Commons Attribution 4.0 License.

$\tau = 3.42$ ms, and normal stress ratio $\Psi = 0.24$. By rotating the plate at a speed of $\Omega \in O(10 \text{ rad s}^{-1})$, the authors observed an indent of size $2a \approx 0.2$ mm forming on the liquid bridge's free surface, which tended to propagate toward the bridge center (Fig. 7). The indent propagation caused the liquid bridge neck radius R to decay in a power-law fashion, i.e., $R(t) \propto t^{-\beta}$ (Fig. 8), where β is the power-law index. The indent could even pinchoff the liquid bridge at a sufficiently high $\Omega \in O(100 \text{ rad s}^{-1})$, as illustrated in Fig. 7. The indentation phenomenon of the silicone oil bridge closely resembled the edge fracture of silicone oil photographically captured by Hutton [3] (see Fig. 1), leading to the authors' supposition that their observations share the same underlying physics as edge fracture.

By dimensional analysis, Chan *et al.* [11] argued that the indentation process was solely governed by the Tanner number Tn. At that time, it was unclear what the characteristic length scale was and whether the first or second normal stress difference caused the indentation phenomenon. Hence, they used the neck radius R as the characteristic length scale and neglected the normal stress ratio Ψ in their definition of Tn. They also neglected the factor of two. For the sake of consistency, however, we shall adhere to the definition of Tn as given in Eq. (1) and use it to reinterpret the results of Chan *et al.* [11] Using the indentation size $2a$ as the characteristic length scale, Tn can be expressed based on the parameters of the three-mode Giesekus model as

$$\text{Tn} = \Psi \tau \eta_0 \frac{R^2 \Omega^2}{a^2} \frac{a}{\Gamma}. \tag{19}$$

For a typical $R \in O(1 \text{ mm})$ and $\Omega \geq O(10 \text{ rad s}^{-1})$, Tn $\geq O(1)$, satisfying the edge fracture criterion given in Eq. (14), supporting the author's supposition that the indentation phenomenon was caused by edge fracture.

Chan *et al.* [11] also performed finite element simulations using the three-model Giesekus model to provide further evidence of edge fracture. They varied the mobility parameter α in the constitutive model, effectively changing the model fluid's normal stress ratio Ψ. Changing α would also change the shear thinning behavior of the fluid; however, as the focus was on the indent formation process during which the shear rate was $\dot{\gamma} \approx R_p \Omega / H \in O(100 \text{ s}^{-1})$, the shear thinning effect could safely be neglected. The results of Chan *et al.* showed that the indent formation speed was positively correlated to the magnitude of N_2, but not N_1, on the indentation tip. Hence, like edge fracture, the indentation process was driven by N_2. Furthermore, the action of N_2 was to compress the indent while pulling it radially inward toward to liquid bridge center, agreeing with the theoretical analysis of edge fracture by Huilgol *et al.* [6]
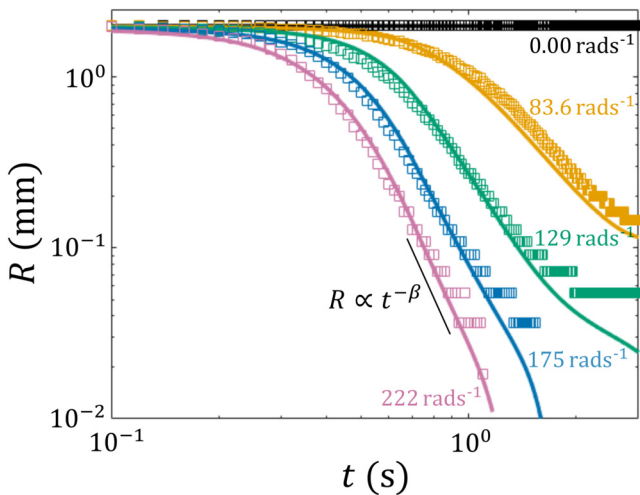

FIG. 8. Radius evolution $R(t)$ of silicone oil bridges of $H = 2.5$ mm under different rotational speeds Ω. Symbols: experimental measurements. Solid lines: numerical predictions by the three-mode Giesekus model. Reproduced with permission from Chan *et al.*, Proc. Natl. Acad. Sci. U.S.A. **118**(24), e2104790118 (2021). 2021 Author(s), licensed under a Creative Commons Attribution 4.0 License.

B. Dynamic similarity and scaling of edge fracture

The dimensional analysis by Chan *et al.* [11] predicted that the edge fracture of the liquid bridge made of silicone oil was solely governed by the Tanner number Tn. For two viscoelastic liquid bridges, as long as their Tn are the same,
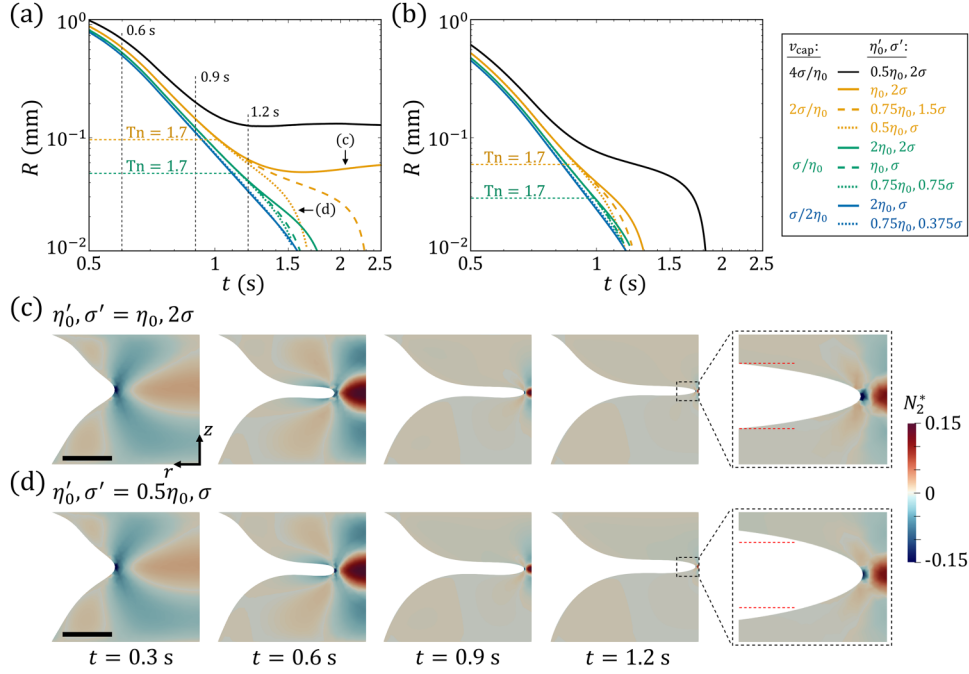
FIG. 9. Simulated edge fracture dynamics of liquid bridges with different viscosity η_0' and interfacial tension Γ'. [(a) and (b)] Radius evolution $R(t)$ of liquid bridges with $H = 2.5$ mm subjected to a rotational speed Ω of (a) 170 and (b) 220 rad s^{-1}. Each color represents one of the four capillary velocities $v_{cap} \equiv \Gamma'/\eta_0'$ shown in the right box. [(c) and (d)] Distributions of the dimensionless second normal stress difference $N_2^* \equiv N_2/\eta_0\Omega$ of liquid bridges with the same v_{cap} subject to $\Omega = 170$ rad s^{-1}, corresponding to the two orange curves labeled (c) and (d) with arrows in (a). Scale bar: 1 mm. Reproduced with permission from Chan *et al.*, Proc. Natl. Acad. Sci. U.S.A., **118**(24), e2104790118 (2021). 2021 Author(s), licensed under a Creative Commons Attribution 4.0 License.

their edge fracture dynamics will be the same. Verifying such a dynamic similarity [80] requires showing that the edge fracture process only depends on the Tanner number Tn. To provide more evidence to support their dimensional analysis, the authors systematically varied in the Giesekus model the viscosity from η_0 to η_0' and interfacial tension from Γ to Γ' while keeping the relaxation time τ and mobility parameter α (hence the normal stress ratio Ψ) the same. Their simulation results showed that as long as the capillary velocity $v_{cap} \equiv \Gamma'/\eta_0'$ of the liquid bridge was the same, $R(t)$ would overlap until Tn became lower than a critical value of $\mathrm{Tn}_c = 1.7 \in O(1)$ [Figs. 9(a) and 9(b)]. The distributions of the dimensionless second normal stress difference $N_2^* \equiv N_2/\eta_0'\Omega$ were seemingly indistinguishable among the liquid bridges as well for $\mathrm{Tn} > \mathrm{Tn}_c$, [Figs. 9(c) and 9(d)]. Besides simulation, Chan *et al.* performed additional liquid bridge experiments using silicone oils with the same interfacial tension Γ but different viscosity η_0 and relaxation time τ. Recall that the authors used $\mathrm{Tn}/2\Psi|_{a=R}$ as their Tanner number. Hence, the normal stress ratio Ψ of those silicone oils was not reported; nonetheless, from the values reported by Keentok and Xue [7], Ψ of those silicone oils was likely the same. Plotting the power-law index β versus $\mathrm{Tn}/2\Psi$ with the plate radius R_p as the characteristic length scale, the data points were seen to collapse onto a single curve, providing further evidence to support the dimensional analysis prediction regarding the sole dependence of Tn.

On the other hand, the experimental and simulation results of Chan *et al.* [11] showed that the liquid bridge radius exhibited power-law decay behavior $R(t) \propto t^{-\beta}$ during fracture. Considering an arbitrary change in time $t \to \mu t$, the

ratio $R(\mu t)/R(t) = \mu^{-\beta}$ is independent of t, i.e., R differs only by a constant factor when viewed at a different time scale. Such self-similarity hinted that the edge fracture process might be scale-invariant [80], which led the authors to anticipate that a similarity solution might be constructed to explain the power-law decay behavior of $R(t)$. If such a solution exists, rheological quantities such as the second normal stress difference N_2 could be obtained simply by tracking the power-law index β.

C. Beyond weak viscoelasticity

Besides the weakly viscoelastic silicone oils, the fracture of liquid bridges made of fluids having different levels of rheological complexity was also reported. Chan *et al.* [12] considered a dilute solution of high molecular weight polystyrene dissolved in oligomeric styrene, which is a Boger fluid with an almost constant shear viscosity $\eta_0 = 43.9$ Pa s, relaxation time $\tau = 5.29$ s, and interfacial tension $\Gamma = 40.5$ mN m^{-1}. The authors identified by dimensional analysis that the liquid bridge deformation depended on two dimensionless numbers. First, there was the Tanner number $\mathrm{Tn}/\Psi = \tau\eta_0 R\Omega^2/\Gamma$. Like their previous study, the authors did not include Ψ and used R as the characteristic length scale in their definition of the Tanner number; in fact, they could not obtain Ψ by shear rheometry since its value is very close to zero for Boger fluids [7]. Then, there was the elastocapillary number $\mathrm{Ec} = \tau\Gamma/\eta_0 R$, typically seen in the context of exponential self-thinning of viscoelastic fluid threads [81]. By inspecting the dependence of $\mathrm{Tn}/2\Psi$ and Ec on R, the authors speculated that the liquid bridge would thin

exponentially over time as R became sufficiently small. They observed such behavior for $\Omega \in O(1 \text{ rad s}^{-1})$. Complementary finite element simulation revealed that torsion induced a negative N_2 at the liquid bridge's neck, similar to edge fracture, bringing the bridge to the elastocapillary thinning state sooner. As a side note, such a phenomenon may be used to estimate the order of magnitude of Ψ for the Boger fluid. Assuming that $R \in O(1 \text{ mm})$, $a \in O(0.1 \text{ mm})$, and $\text{Tn} \in O(1)$ will give $\Psi \in O(0.01)$, which agrees with a previous report that $\Psi = 0.01 \pm 0.01$ for a Boger fluid made of polyisobutylene dissolved in oligomeric polybutene [82]. For $\Omega \in O(10 \text{ rad s}^{-1})$, helical wrinkles could be observed on the liquid bridge surface as it was twisted. The bridge's top and bottom fluid reservoirs were seen to approach each other, leading to an elastic instability before the bridge could break up. The process was visually similar to the Weissenberg rod-climbing phenomenon [17] but with the solid rod being replaced with a "liquid rod." For $\Omega \in O(100 \text{ rad s}^{-1})$, the thinning speed of the liquid rod becames faster than the climbing speed of the fluid reservoirs, and the liquid bridge breakup was observed.

Subsequently, Chan *et al.* [13] studied the edge fracture of liquid bridges made of a thixotropic elastoviscoplastic (TEVP) thermal paste, demonstrating that fracture can also be used to break TEVP bridges. By dimensional analysis, they predicted that when $\text{Tn} \in O(1)$, the Bingham number would be $\text{Bn} \in O(10^{-2})$. Hence, the effect of plasticity is negligible when edge fracture occurs. Complementary finite element simulation using a phenomenological TEVP constitutive model verified their prediction.

VI. SUMMARY AND OUTLOOK

Alongside the Weissenberg rod-climbing effect [17] and the elastocapillary self-thinning of elastic fluid threads [81], edge fracture is one of the few viscoelastic instabilities with a solid theoretical basis supported by extensive experiments. Previous research on edge fracture has primarily focused on mitigating the phenomenon. Techniques such as thin-gap rheometry and geometries such as the guard ring assembly and CPP fixture have been developed for this purpose. However, there is still a lack of research on harnessing the fracture phenomenon. Additionally, the rheology community has neglected promising mitigation strategies that merit further investigation. The study of edge fracture is full of opportunities to be explored and problems to be solved.

A. Edge fracture of non-Brownian suspensions

Edge fracture can also occur in non-Brownian suspensions, such as greases and pastes, which play a critical role in various industrial applications such as food engineering, additive manufacturing, and electronic packaging. Despite their importance, most research on edge fractures has focused on polymeric fluids. For instance, the most recent theory of fracture, developed by Hemingway and Fielding [8], is based on the Johnson–Segalman and Giesekus constitutive models for polymeric fluids. Hence, it is unclear whether this theory can be applied to suspensions. Although some studies on edge fractures in suspensions exist, most of them focus on yield stress fluids. Furthermore, those studies are mainly descriptive [83,84], potentially because of the difficulty of measuring normal stress differences due to interference from the material's yield stress. Recently, a new method for measuring normal stress in yield stress fluids using the large amplitude oscillatory shear test at low frequency has been proposed by de Cagny *et al.* [22]. This method is applicable in any laboratory with a stress-controlled rotational rheometer and could be used to study edge fractures in suspensions. Additionally, Tanner and Dai [85] suggested that a stability analysis using the Reiner–Rivlin model could provide new insights into the edge fracture of suspensions. In their subsequent studies [86,87], the authors further proposed using the Thompson–de Souza Mendes model [88] and a two-part composite variant composed of the Thompson–de Souza Mendes model and a multimode Oldroyd-B model to describe non-Brownian suspensions; those models might also be useful for the stability analysis.

B. Liquid metal sealing

As discussed in Sec. IV A, sealing the fluid sample's free surface with the nontoxic liquid metal galinstan can delay edge fracture [16]. However, one point deserves attention. The critical Tanner number Tn_c at which fracture occurred for the silicone oil sealed with galinstan was estimated to be $O(10)$, deviating from the edge fracture theories, which predict $\text{Tn}_c \in O(1)$. One possible explanation is that the centrifugal force exerted by the liquid metal on the silicone oil could oppose the second normal stress difference, pulling the fracture backward as it develops. Another explanation is that as the interfacial tension of the free surface increases, the fracture's penetration depth will decrease, suppressing its negative influence on shear rheometry. To our knowledge, there has been no systematic experimental study of this phenomenon. One piece of evidence comes from Hemingway and Fielding [8]; their phase-field simulation showed that increasing the interfacial tension can lead to a lower penetration depth of the fracture (see the state diagram in Fig. 6). Another indirect evidence comes from Chan *et al.* [see Fig. 9(a), black and orange solid lines], who showed by simulations that halving the viscosity while keeping the interfacial tension constant could increase the neck radius R_c at which edge fracture halts in the liquid bridge [11]. According to Eq. (19), assuming that Tn_c is a constant when fracture halts will give the relation $R_c^2 \propto \Gamma/\eta_0$. The effect of halving η_0 is the same as doubling Γ. Hence, increasing Γ shall lead to a larger R_c, i.e., a smaller penetration depth of the fracture. From a physical point of view, such an explanation makes sense, as fracturing is a process of creating new surfaces and increasing surface energy [89]. Given that the work done by the second normal stress difference N_2 is the same, as Γ increases, the surface area that can be created will be more limited. Experiments and simulations are needed to test which explanation is true. Nonetheless, it is expected that the galinstan sealing method can be applied with the CPP fixture, extending the measurable range of the shear rate even further. Overfilling the fluid sample in the CPP fixture can

ensure that the liquid metal will completely wet the fluid sample.

C. Dynamics of edge fracture

The torsional instability of liquid bridges studied by Chan *et al.* [11] provided insights regarding the dynamics of edge fracture. The fracture process solely depends on the Tanner number Tn, implying dynamic similarity. The neck radius $R(t)$ of the liquid bridge undergoing fracture showed power-law decay, suggesting self-similarity and scale invariance of the fracture process. Nonetheless, there is insufficient information on whether edge fracture is truly scale-invariant. Verifying so requires demonstrating the self-similarity of the velocity and stress fields during fracture propagation.

In turn, this requires deriving a simple physical model, which would still incorporate the necessary physics to predict the onset and subsequent evolution of edge fracture. The simplified Couette geometry studied by Hemingway and Fielding [8] could be an excellent candidate for this purpose. The fluid is sheared in a planar slab at a rate $\dot{\gamma}$. This geometry approximates the cone-and-plate and parallel-plate fixtures when the plate radius is much larger than the cone angle or gap size. Additional assumptions can be made in favor of reducing the flow parameters. Inertia can be neglected, assuming creeping flow. The same holds for gravity. A fully developed flow can be assumed in the flow direction. The three-phase contact lines formed by the fluid, the surrounding air, and the solid plates can be considered pinned. This means that the contact lines are not allowed to move tangentially to the wall, and the contact angle is calculated implicitly from the flow field. The viscosity of the surrounding air can also be neglected. Finally, the quasilinear lower convected Maxwell model can be used to describe the fluid sample's rheology. This constitutive equation predicts a nonzero N_2, featuring only two rheological parameters: the relaxation time τ and the polymeric viscosity η_p. Moreover, the lower convected Maxwell mode predicts strong normal stresses that increase quadratically with increasing shear rate, which would prolong the power-law fracture propagation regime. Under these assumptions, the problem shall be governed solely by the Tanner number Tn. Although the problem remains three-dimensional, all flow variables (velocity, pressure, stresses, and free surface height) depend only on the gradient and vorticity directions. The simplified system of partial differential equations can be solved numerically to obtain the minimum sample radius R versus time t and check whether it depends solely on Tn. Assuming that R is the only length scale, the flow variables around the indent can be rescaled at different time instants and compared to each other to see whether edge fracture is self-similar. A potential characteristic length scale a_s for such a rescaling procedure may be obtained by requiring the governing dimensionless number, in this case, Tn, to be a constant during the fracture process, giving $a_s \propto \Gamma/|N_2|$. A complementary approach would be to describe the fluid as an elastic solid, assuming dominant elastic effects and negligible stress relaxation. Eggers *et al.* [90] recently implemented this idea

to derive a similarity solution for the elastocapillary breakup of polymeric threads.

D. Functional dispensing nozzles

Torsion can induce edge fracture and destabilize viscoelastic liquid bridges without extending them, avoiding the stringing problem. This may help improve the efficiency of processes such as 3D printing and electronic packaging that require rheologically complex fluids to be dispensed quickly and cleanly. Also, this may allow materials previously thought unprintable, such as those with high elasticity or high yield stress, to be printed. However, from an engineering point of view, designing a fluid dispensing nozzle that can rotate can be difficult. Nonetheless, such nozzle designs have already been proposed for 3D printing. For instance, Raney *et al.* [91] employed a rotatable nozzle to control the fiber orientation in their 3D-printed fiber-epoxy composite materials. On the other hand, Löffler and Koch [92] designed a nozzle with a slot-shaped opening to vary the linewidth of the dispensed fluid without having to use multiple nozzles. Potentially, these designs can be used to test the idea of harnessing edge fracture to break liquid bridges for dispensing purposes.

AUTHOR DECLARATIONS
Conflict of Interest

The authors have no conflicts to disclose.

DATA AVAILABILITY

Data sharing is not applicable to this article as no new data were created or analyzed in this study.

REFERENCES

[1] Hutton, J. F., "Fracture of liquids in shear," Nature **200**, 646–648 (1963).
[2] Hutton, J. F., "The fracture of liquids in shear: The effects of size and shape," Proc. R. Soc. London, Ser. A **287**, 222–239 (1965).
[3] Hutton, J. F., "Fracture and secondary flow of elastic liquids," Rheol. Acta **8**, 54–59 (1969).
[4] Tanner, R. I., and M. Keentok, "Shear fracture in cone-plate rheometry," J. Rheol. **27**, 47–57 (1983).
[5] Lee, C. S., B. C. Tripp, and J. J. Magda, "Does N_1 or N_2 control the onset of edge fracture?," Rheol. Acta **31**, 306–308 (1992).
[6] Huilgol, R. R., M. Panizza, and L. E. Payne, "On the rectilinear flow of a second-order fluid and the role of the second normal stress difference in edge fracture in rheometry," J. Non-Newtonian Fluid Mech. **50**, 331–348 (1993).

[7] Keentok, M., and S. C. Xue, "Edge fracture in cone-plate and parallel plate flows," Rheol. Acta **38**, 321–348 (1999).

[8] Hemingway, E. J., and S. M. Fielding, "Edge fracture instability in sheared complex fluids: Onset criterion and possible mitigation strategy," J. Rheol. **63**, 735–750 (2019).

[9] Maklad, O., and R. J. Poole, "A review of the second normal-stress difference; its importance in various flows, measurement techniques, results for various complex fluids and theoretical predictions," J. Non-Newtonian Fluid Mech. **292**, 104522 (2021).

[10] Hemingway, E. J., and S. M. Fielding, "Interplay of edge fracture and shear banding in complex fluids," J. Rheol. **64**, 1147–1159 (2020).

[11] Chan, S. T., F. P. A. van Berlo, H. A. Faizi, A. Matsumoto, S. J. Haward, P. D. Anderson, and A. Q. Shen, "Torsional fracture of viscoelastic liquid bridges," Proc. Natl. Acad. Sci. U.S.A. **118**, e2104790118 (2021).

[12] Chan, S. T., S. Varchanis, S. J. Haward, and A. Q. Shen, "Torsional instability of constant viscosity elastic liquid bridges," Soft Matter **18**, 1965–1977 (2022).

[13] Chan, S. T., S. Varchanis, A. Q. Shen, and S. J. Haward, "Edge fracture of thixotropic elastoviscoplastic liquid bridges," PNAS Nexus **2**, pgad042 (2023).

[14] Poole, R. J., "The Deborah and Weissenberg numbers," Rheol. Bull. **53**, 32–39 (2012).

[15] Oldroyd, J. G., "On the formulation of rheological equations of state," Proc. R. Soc., Ser. A **200**, 523–541 (1950).

[16] Chan, S. T., S. J. Haward, and A. Q. Shen, "Prevention of edge fracture using a non-toxic liquid metal sealant," Phys. Fluids **35**(1), 011704 (2022).

[17] Boger, D. V., and K. Walters, *Rheological Phenomena in Focus* (Elsevier, Amsterdam, 1993).

[18] Denn, M. M., "Issues in viscoelastic fluid mechanics," Annu. Rev. Fluid Mech. **22**, 13–32 (1990).

[19] Hill, D. A., T. Hasegawa, and M. M. Denn, "On the apparent relation between adhesive failure and melt fracture," J. Rheol. **34**, 891–918 (1990).

[20] Fernández, M., A. Santamarıa, A. Muñoz-Escalona, and L. Méndez, "A striking hydrodynamic phenomenon: Split of a polymer melt in capillary flow," J. Rheol. **45**, 595–602 (2001).

[21] Phan-Thien, N., and R. I. Tanner, "A new constitutive equation derived from network theory," J. Non-Newtonian Fluid Mech. **2**, 353–365 (1977).

[22] De Cagny, H., M. Fazilati, M. Habibi, M. M. Denn, and D. Bonn, "The yield normal stress," J. Rheol. **63**, 285–290 (2019).

[23] Olmsted, P. D., "Perspectives on shear banding in complex fluids," Rheol. Acta **47**, 283–300 (2008).

[24] Manneville, S., "Recent experimental probes of shear banding," Rheol. Acta **47**, 301–318 (2008).

[25] Schall, P., and M. Van Hecke, "Shear bands in matter with granularity," Annu. Rev. Fluid Mech. **42**, 67–88 (2010).

[26] Wang, S. Q., S. Ravindranath, and P. E. Boukany, "Homogeneous shear, wall slip, and shear banding of entangled polymeric liquids in simple-shear rheometry: A roadmap of nonlinear rheology," Macromolecules **44**, 183–190 (2011).

[27] Fielding, S. M., "Shear banding in soft glassy materials," Rep. Prog. Phys. **77**, 102601 (2014).

[28] Divoux, T., M. A. Fardin, S. Manneville, and S. Lerouge, "Shear banding of complex fluids," Annu. Rev. Fluid Mech. **48**, 81–103 (2016).

[29] Wang, S. Q., "From wall slip to bulk shear banding in entangled polymer solutions," Macromol. Chem. Phys. **220**, 1800327 (2019).

[30] Germann, N., "Shear banding in semidilute entangled polymer solutions," Curr. Opin. Colloid Interface Sci. **39**, 1–10 (2019).

[31] Tapadia, P., and S. Q. Wang, "Yieldlike constitutive transition in shear flow of entangled polymeric fluids," Phys. Rev. Lett. **91**, 198301 (2003).

[32] Tapadia, P., and S. Q. Wang, "Nonlinear flow behavior of entangled polymer solutions: Yieldlike entanglement-disentanglement transition," Macromolecules **37**, 9083–9095 (2004).

[33] Inn, Y. W., K. F. Wissbrun, and M. M. Denn, "Effect of edge fracture on constant torque rheometry of entangled polymer solutions," Macromolecules **38**, 9385–9388 (2005).

[34] Tapadia, P., and S. Q. Wang, "Direct visualization of continuous simple shear in non-Newtonian polymeric fluids," Phys. Rev. Lett. **96**, 016001 (2006).

[35] Hu, Y. T., L. Wilen, A. Philips, and A. Lips, "Is the constitutive relation for entangled polymers monotonic?," J. Rheol. **51**, 275–295 (2007).

[36] Sui, C., and G. B. McKenna, "Instability of entangled polymers in cone and plate rheometry," Rheol. Acta **46**, 877–888 (2007).

[37] Ravindranath, S., and S. Q. Wang, "Steady state measurements in stress plateau region of entangled polymer solutions: Controlled-rate and controlled-stress modes," J. Rheol. **52**, 957–980 (2008).

[38] Hu, Y. T., "Steady-state shear banding in entangled polymers?," J. Rheol. **54**, 1307–1323 (2010).

[39] Skorski, S., and P. D. Olmsted, "Loss of solutions in shear banding fluids driven by second normal stress differences," J. Rheol. **55**, 1219–1246 (2011).

[40] Ravindranath, S., Y. Wang, P. Boukany, and X. Li, "Letter to the editor: Cone partitioned plate (CPP) vs circular couette," J. Rheol. **56**, 675–681 (2012).

[41] Hu, Y. T., "Response to: CPP vs circular couette," J. Rheol. **56**, 683–686 (2012).

[42] Li, Y., M. Hu, G. B. McKenna, C. J. Dimitriou, G. H. McKinley, R. M. Mick, D. C. Venerus, and L. A. Archer, "Flow field visualization of entangled polybutadiene solutions under nonlinear viscoelastic flow conditions," J. Rheol. **57**, 1411–1428 (2013).

[43] Wang, S. Q., G. Liu, S. Cheng, P. E. Boukany, Y. Wang, and X. Li, "Letter to the editor: Sufficiently entangled polymers do show shear strain localization at high enough Weissenberg numbers," J. Rheol. **58**, 1059–1069 (2014).

[44] Li, Y., M. Hu, G. B. McKenna, C. J. Dimitriou, G. H. McKinley, R. M. Mick, D. C. Venerus, and L. A. Archer, "Response to: Sufficiently entangled polymers do show shear strain localization at high enough Weissenberg numbers," J. Rheol. **58**, 1071–1082 (2014).

[45] Fielding, S. M., and P. D. Olmsted, "Kinetics of the shear banding instability in startup flows," Phys. Rev. E **68**, 036313 (2003).

[46] Fielding, S. M., and P. D. Olmsted, "Early stage kinetics in a unified model of shear-induced demixing and mechanical shear banding instabilities," Phys. Rev. Lett. **90**, 224501 (2003).

[47] Fielding, S. M., and P. D. Olmsted, "Flow phase diagrams for concentration-coupled shear banding," Eur. Phys. J. E **11**, 65–83 (2003).

[48] Cromer, M., M. C. Villet, G. H. Fredrickson, and L. G. Leal, "Shear banding in polymer solutions," Phys. Fluids **25**, 051703 (2013).

[49] Cromer, M., G. H. Fredrickson, and L. G. Leal, "A study of shear banding in polymer solutions," Phys. Fluids **26**, 063101 (2014).

[50] Peterson, J. D., M. Cromer, G. H. Fredrickson, and L. G. Leal, "Shear banding predictions for the two-fluid rolie-poly model," J. Rheol. **60**, 927–951 (2016).

[51] Burroughs, M. C., Y. Zhang, A. M. Shetty, C. M. Bates, L. G. Leal, and M. E. Helgeson, "Flow-induced concentration nonuniformity and shear banding in entangled polymer solutions," Phys. Rev. Lett. **126**, 207801 (2021).

[52] Li, Y., and G. B. McKenna, "Startup shear of a highly entangled polystyrene solution deep into the nonlinear viscoelastic regime," Rheol. Acta **54**, 771–777 (2015).

[53] Aral, B. K., and D. M. Kalyon, "Effects of temperature and surface roughness on time-dependent development of wall slip in steady torsional flow of concentrated suspensions," J. Rheol. **38**, 957–972 (1994).

[54] Johnson, Jr., M. W., and D. Segalman, "A model for viscoelastic fluid behavior which allows non-affine deformation," J. Non-Newtonian Fluid Mech. **2**, 255–270 (1977).

[55] Giesekus, H., "A simple constitutive equation for polymer fluids based on the concept of deformation-dependent tensorial mobility," J. Non-Newtonian Fluid Mech. **11**, 69–109 (1982).

[56] Giesekus, H., "Stressing behaviour in simple shear flow as predicted by a new constitutive model for polymer fluids," J. Non-Newtonian Fluid Mech. **12**, 367–374 (1983).

[57] Helgeson, M. E., P. A. Vasquez, E. W. Kaler, and N. J. Wagner, "Rheology and spatially resolved structure of cetyltrimethylammonium bromide wormlike micelles through the shear banding transition," J. Rheol. **53**, 727–756 (2009).

[58] Berret, J. F., G. Porte, and J. P. Decruppe, "Inhomogeneous shear flows of wormlike micelles: A master dynamic phase diagram," Phys. Rev. E **55**, 1668 (1997).

[59] Connelly, R. W., and J. Greener, "High-shear viscometry with a rotational parallel-disk device," J. Rheol. **29**, 209–226 (1985).

[60] Pipe, C. J., T. S. Majmudar, and G. H. McKinley, "High shear rate viscometry," Rheol. Acta **47**, 621–642 (2008).

[61] Davies, G. A., and J. R. Stokes, "Thin film and high shear rheology of multiphase complex fluids," J. Non-Newtonian Fluid Mech. **148**, 73–87 (2008).

[62] Andablo-Reyes, E., R. Hidalgo-Álvarez, and J. De Vicente, "A method for the estimation of the film thickness and plate tilt angle in thin film misaligned plate–plate rheometry," J. Non-Newtonian Fluid Mech. **165**, 1419–1421 (2010).

[63] Schweizer, T., and A. Bardow, "The role of instrument compliance in normal force measurements of polymer melts," Rheol. Acta **45**, 393–402 (2006).

[64] Grizzuti, N., P. Moldenaers, M. Mortier, and J. Mewis, "On the time-dependency of the flow-induced dynamic moduli of a liquid crystalline hydroxypropylcellulose solution," Rheol. Acta **32**, 218–226 (1993).

[65] Sigillo, I., and N. Grizzuti, "The effect of molecular weight on the steady shear rheology of lyotropic solutions. A phenomenological study," J. Rheol. **38**, 589–599 (1994).

[66] Palathoti, S. R., V. O. Otitolaiye, R. Mahfud, and M. Al Rawahi, "Impacts of mercury exposure on human health, safety and environment: Literature review and bibliometric analysis (1995 to 2021)," Int. J. Occup. Saf. Health **12**, 336–352 (2022).

[67] Liu, T., P. Sen, and C. J. Kim, "Characterization of nontoxic liquid-metal alloy galinstan for applications in microdevices," J. Microelectromech. Syst. **21**, 443–450 (2011).

[68] Mall-Gleissle, S. E., W. Gleissle, G. H. McKinley, and H. Buggisch, "The normal stress behaviour of suspensions with viscoelastic matrix fluids," Rheol. Acta **41**, 61–76 (2002).

[69] Gleissle, W., "Druckverteilung im spalt eines kegel-platte-rheometers bei der scherung viskoelastischer flüssigkeiten mit hohen schergeschwindigkeiten," Rheol. Acta **15**, 305–316 (1976).

[70] Pieper, S., and H. J. Schmid, "Guard ring induced distortion of the steady velocity profile in a parallel plate rheometer," Appl. Rheol. **26**, 18–24 (2016).

[71] Snijkers, F., and D. Vlassopoulos, "Cone-partitioned-plate geometry for the ares rheometer with temperature control," J. Rheol. **55**, 1167–1186 (2011).

[72] Costanzo, S., G. Ianniruberto, G. Marrucci, and D. Vlassopoulos, "Measuring and assessing first and second normal stress differences of polymeric fluids with a modular cone-partitioned plate geometry," Rheol. Acta **57**, 363–376 (2018).

[73] Meissner, J., R. W. Garbella, and J. Hostettler, "Measuring normal stress differences in polymer melt shear flow," J. Rheol. **33**, 843–864 (1989).

[74] Schweizer, T., "Measurement of the first and second normal stress differences in a polystyrene melt with a cone and partitioned plate tool," Rheol. Acta **41**, 337–344 (2002).

[75] Schweizer, T., "Comparing cone-partitioned plate and cone-standard plate shear rheometry of a polystyrene melt," J. Rheol. **47**, 1071–1085 (2003).

[76] Schweizer, T., "A quick guide to better viscosity measurements of highly viscous fluids," Appl. Rheol. **14**, 197–201 (2004).

[77] Williams, S. J., C. Park, and S. T. Wereley, "Advances and applications on microfluidic velocimetry techniques," Microfluid. Nanofluidics **8**, 709–726 (2010).

[78] Li, X., and S.-Q. Wang, "Elastic yielding after step shear and during laos in the absence of meniscus failure," Rheol. Acta **49**, 985–991 (2010).

[79] Schweizer, T., and W. Schmidheiny, "A cone-partitioned plate rheometer cell with three partitions (CPP3) to determine shear stress and both normal stress differences for small quantities of polymeric fluids," J. Rheol. **57**, 841–856 (2013).

[80] Barenblatt, G. I., *Scaling, Self-Similarity, and Intermediate Asymptotics: Dimensional Analysis and Intermediate Asymptotics* (Cambridge University, Cambridge, 1996), p. 14.

[81] McKinley, G. H., "Visco-elasto-capillary thinning and break-up of complex fluids," Rheol. Rev. **3**, 1–48 (2005).

[82] Magda, J. J., J. Lou, S. G. Baek, and K. L. DeVries, "Second normal stress difference of a Boger fluid," Polymer **32**, 2000–2009 (1991).

[83] Hutton, J. F., "On using the Weissenberg rheogoniometer to measure normal stresses in lubricating greases as examples of materials which have a yield stress," Rheol. Acta **14**, 979–992 (1975).

[84] Magnin, A., and J. M. Piau, "Shear rheometry of fluids with a yield stress," J. Non-Newtonian Fluid Mech. **23**, 91–106 (1987).

[85] Tanner, R. I., and S. Dai, "Edge fracture in non-colloidal suspensions," J. Non-Newtonian Fluid Mech. **272**, 104171 (2019).

[86] Tanner, R. I., and S. Dai, "Modelling inelastic non-colloidal suspensions," Rheol. Acta **60**, 643–652 (2021).

[87] Tanner, R. I., and S. Dai, "Forming a composite model for non-Brownian suspensions," Phys. Fluids **34**, 083304 (2022).

[88] Thompson, R. L., and P. R. de Souza Mendes, "A constitutive model for non-Newtonian materials based on the persistence-of-straining tensor," Meccanica **46**, 1035–1045 (2011).

[89] Griffith, A. A., "The phenomena of rupture and flow in solids," Philos. Trans. R. Soc., A **221**, 163–198 (1921).

[90] Eggers, J., M. A. Herrada, and J. H. Snoeijer, "Self-similar breakup of polymeric threads as described by the Oldroyd-B model," J. Fluid Mech. **887**, A19 (2020).

[91] Raney, J. R., B. G. Compton, J. Mueller, T. J. Ober, K. Shea, and J. A. Lewis, "Rotational 3D printing of damage-tolerant composites with programmable mechanics," Proc. Natl. Acad. Sci. U.S.A. **115**, 1198–1203 (2018).

[92] Löffler, R., and M. Koch, "Innovative extruder concept for fast and efficient additive manufacturing," IFAC-PapersOnLine **52**, 242–247 (2019).